

# A new Python library to analyse skeleton images confirms malaria parasite remodelling of the red blood cell membrane skeleton

Juan Nunez-Iglesias <sup>Corresp., 1</sup>, Adam J Blanch <sup>2</sup>, Oliver Looker <sup>2</sup>, Matthew W Dixon <sup>2</sup>, Leann Tilley <sup>2</sup>

<sup>1</sup> Melbourne Bioinformatics, The University of Melbourne, Australia

<sup>2</sup> Department of Biochemistry and Molecular Biology, Bio21 Institute, University of Melbourne, Melbourne, Australia

Corresponding Author: Juan Nunez-Iglesias  
Email address: juan.n@unimelb.edu.au

We present Skan (Skeleton analysis), a Python library for the analysis of the skeleton structures of objects. It was inspired by the “analyse skeletons” plugin for the Fiji image analysis software, but its extensive Application Programming Interface (API) allows users to examine and manipulate any intermediate data structures produced during the analysis. Further, its use of common Python data structures such as SciPy sparse matrices and pandas data frames opens the results to analysis within the extensive ecosystem of scientific libraries available in Python. We demonstrate the validity of Skan’s measurements by comparing its output to the established Analyze Skeletons Fiji plugin, and, with a new scanning electron microscopy (SEM)-based method, we confirm that the malaria parasite *Plasmodium falciparum* remodels the host red blood cell cytoskeleton, increasing the average distance between spectrin-actin junctions.

# A new Python library to analyse skeleton images confirms malaria parasite remodelling of the red blood cell membrane skeleton

Juan Nunez-Iglesias<sup>1,2</sup>, Adam J. Blanch<sup>1,3</sup>, Oliver Looker<sup>3</sup>, Matthew W. Dixon<sup>3</sup>, and Leann Tilley<sup>3</sup>

<sup>1</sup>Co-first author

<sup>2</sup>Melbourne Bioinformatics, The University of Melbourne, Australia

<sup>3</sup>Department of Biochemistry and Molecular Biology, Bio21 Institute, The University of Melbourne, Australia

Corresponding author:

Juan Nunez-Iglesias<sup>2</sup>

Email address: [juan.n@unimelb.edu.au](mailto:juan.n@unimelb.edu.au)

## ABSTRACT

We present Skan (Skeleton analysis), a Python library for the analysis of the skeleton structures of objects. It was inspired by the “analyse skeletons” plugin for the Fiji image analysis software, but its extensive Application Programming Interface (API) allows users to examine and manipulate any intermediate data structures produced during the analysis. Further, its use of common Python data structures such as SciPy sparse matrices and pandas data frames opens the results to analysis within the extensive ecosystem of scientific libraries available in Python. We demonstrate the validity of Skan’s measurements by comparing its output to the established Analyze Skeletons Fiji plugin, and, with a new scanning electron microscopy (SEM)-based method, we confirm that the malaria parasite *Plasmodium falciparum* remodels the host red blood cell cytoskeleton, increasing the average distance between spectrin-actin junctions.

## INTRODUCTION

Skeletons are single-pixel thick representations of networks within an image, and have wide application to understanding the structural properties of objects. For example, skeletons have been used to model human poses, neuronal morphology, nanofibre structure, road networks, kidney development, and vascular networks, among others (Yim et al., 2000; Sundar et al., 2003; Bas and Erdogmus, 2011; Yuan et al., 2009; Morales-Navarrete et al., 2015; Sambaer et al., 2011). These applications include both 2D and 3D images, and often 3D images collected over time, underscoring the need for skeleton analysis software to support multiple imaging modalities and dimensionality.

In this paper, we report Skan, a Python library that produces graphs and branch statistics from skeleton images. Skan is written in Python using the Numba just-in-time (JIT) compiler (Lam et al., 2015) for performance-critical code, including graph building and graph statistics computation. The source code is available at <https://github.com/jni/skan> (under a BSD 3-clause license), and we encourage readers to contribute code or raise GitHub issues where they require additional functionality to meet their needs.

Skan works transparently with images of any dimensionality, allowing the analysis of 2D and 3D skeletons. Out of the box, Skan provides functions to compute the pixel skeleton graph, compute statistics about the branches of the skeleton, and draw skeletons and statistical overlays for 2D images.

The pixel skeleton graph maps which pixel is connected to which others in the skeleton image, as well as the distances between them. This graph is provided in the standard `scipy.sparse.csr_matrix` sparse matrix format, enabling further analysis using common tools for graph and array manipulation in the scientific Python ecosystem.

44 From this graph, we can compute statistics about the branches of the skeleton, defined as junction-  
45 junction and junction-endpoint paths in the pixel skeleton graph. These statistics include average branch  
46 length, branch type, branch curvature, branch endpoints, branch euclidean length, and average image  
47 intensity along the branch. We return these statistics as a pandas DataFrame, the de-facto standard format  
48 for data tables in Python. The table includes the pixel IDs of the branch endpoints, allowing further  
49 analysis of the junction-junction graph. Indeed, increasing the breadth of statistics computed by the  
50 software was the primary motivation for Skan's development.

51 Skan further provides a rudimentary GUI to analyse batches of input images. The output of the  
52 GUI interface is an Excel file, which contains all the above-mentioned statistics, as well as all analysis  
53 parameters, to aid future reproducibility.

54 Because Skan uses common scientific Python data structures internally, it is easy to extend with new  
55 statistics and analyses. The DataFrame of branch statistics follows the "tidy data" paradigm (Wickham,  
56 2014), with each row representing one branch of a skeleton, facilitating downstream analysis, such as  
57 computing summary statistics for each disjoint skeleton in an image.

58 To demonstrate Skan's 3D capabilities, we first compared its output to that of Fiji's Analyze Skeletons  
59 (Arganda-Carreras et al., 2010), applied to a publicly available dataset of neuron skeleton traces. Then, we  
60 used Skan to measure the spectrin cytoskeleton on the cytoplasmic side of the plasma membrane of red  
61 blood cells (RBCs) infected with the malaria parasite *Plasmodium falciparum*, using a new SEM-based  
62 protocol, and confirmed the remodelling of the RBC membrane skeleton by the parasite.

## 63 METHODS

### 64 Analysis of skeleton model from DIADEM challenge

65 We downloaded the olfactory projection neuron 1 (OP-1) model as a SWC file from DIADEM's website  
66 at [http://diademchallenge.org/data\\_set\\_downloads.html](http://diademchallenge.org/data_set_downloads.html), along with its corresponding 3D TIFF image  
67 stack. We then rasterised the model (i.e. converted it from a network of vertex coordinates to a set  
68 of active pixels) by using the Simple Neurite Tracer (Longair et al., 2011) plugin for Fiji, function  
69 "Analysis > Render/Analyze Skeletonized Paths." This produces a 6-connected skeleton path, which  
70 we needed to convert to a (thinner) 26-connected path, so we further skeletonized the raster with the  
71 `morphology.skeletonize3d` function from scikit-image (van der Walt et al., 2014), and saved it  
72 as a compressed TIFF file.

73 Then, we imported this raster image into either Fiji or Python (using Christoph Gohlke's TIFFfile). In  
74 both cases, we manually set the scale to  $9.100602 \times 3.033534 \times 3.033534$   $\mu\text{m}$  per voxel, as documented  
75 on the DIADEM website. In Fiji, we used "Analyze Skeletons" with the "Show detailed info" option  
76 ticked, saved the results to csv, and loaded them into a pandas DataFrame in Python. In Python, we used  
77 `skan.csr.summarise` to produce a corresponding pandas DataFrame for Skan's analysis. Finally,  
78 we used `numpy.histogram` and `matplotlib.pyplot.hist` to produce the histogram in Figure  
79 1.

### 80 Tissue origin and ethics approval

81 This study made use of donated human red blood cells. All experiments were approved by The University  
82 of Melbourne School of Biomedical Sciences, Human Ethics Advisory Group (HEAG), for project titled  
83 "Characterising host cell interactions in the human malaria parasite, *Plasmodium falciparum*", and ethics  
84 ID 1135799. Cells were obtained by a Material Supply Agreement with the Australian Red Cross Blood  
85 Service, agreement number – 17-05VIC-23.

### 86 Sample preparation and SEM imaging

87 To prepare sheared membranes, infected and uninfected red blood cells were attached to 3-Aminopropyl-  
88 triethoxysilane treated glass slides using the lectin erythro-agglutinating phytohemagglutinin (PHA-E)  
89 and sheared in a hypotonic buffer according to a previously established procedure (Shi et al., 2013).  
90 Sheared membranes were immediately fixed with 2.5% glutaraldehyde for 1 h before dehydration in a  
91 series of ethanol:water mixtures of 20, 50, 70, 80, 90, 95 and (3x) 100% ethanol for 5 minutes each and  
92 finally being allowed to dry in air.

93 Dried samples were gold coated on the rotating mount of a Dynavac SC100 sputter coating instrument  
94 for 35 seconds using a 25 mA current, measuring 0.2 nm thickness on the quartz crystal microbalance.

95 The coating procedure was optimised to prevent under- or overcoating which presents problems with the  
96 skeleton trace.

97 SEM images were recorded using the ETD detector (in Optiplan mode) of an FEI Teneo instrument  
98 with a working distance of 5 mm, a beam current of 50 pA and a 2 kV accelerating voltage. Multiple  
99 images at 200-250 k magnification were recorded per individual cell to cover a greater portion of the  
100 membrane.

### 101 **Extraction of skeleton data from SEM images**

102 In our SEM images, the spectrin-actin network appears as bright (raised) patches over dark patches of  
103 background (see Figure 1). We followed a simple approach to trace the midline of the spectrin branches:  
104 smoothing the images, then thresholding them (Sauvola and Pietikäinen, 2000), and finally thinning them  
105 (Zhang and Suen, 1984). The width of the Gaussian smoothing, the window size for thresholding, and the  
106 offset for the thresholding are all parameters of our approach, and are recorded in the results output file of  
107 a skeleton analysis (when using the graphical user interface).

### 108 **Data and code availability**

109 Our code is open source and available at <https://github.com/jni/skan>. Additionally, some scripts used in  
110 analysis are available at <https://github.com/jni/skan-scripts>.

111 We have made the schizont SEM dataset available at the Open Science Framework (OSF), with DOI  
112 10.17605/OSF.IO/SVPFU.

## 113 **RESULTS**

### 114 **Comparison to Fiji's Analyze Skeletons plugin**

115 As a check that our software was producing results consistent with the existing literature on skeleton  
116 analysis, we compared our software's results with that of Fiji's Analyze Skeletons plugin (Arganda-  
117 Carreras et al., 2010). Although the original data from that paper is unavailable (Ignacio Arganda-  
118 Carreras, pers. commun.), we compared the output of our software with that of Analyze Skeletons on a  
119 neuron skeleton from the DIADEM Challenge (<http://diademchallenge.org>) (Figure 1A-B). Both software  
120 packages found the same number of skeleton branches, with very close agreement between the two branch  
121 length distributions (Figure 1C) and branch point locations (Figure 1D). Manual inspection confirmed that  
122 the small differences observed result from the different treatment of branch junctions (see Supplementary  
123 Information).

### 124 **Malaria parasites remodel the red blood cell inner membrane cytoskeleton**

125 Prior studies have shown that infection by *P. falciparum*, the most deadly malaria-causing parasite, results  
126 in changes in the physical properties of the infected red blood cell (iRBC), and that these changes are  
127 associated with an elongation of the spectrin skeleton branches in the inner RBC membrane skeleton  
128 (Shi et al., 2013; Dearnley et al., 2016; Nans et al., 2011). A coarse-grained molecular model suggested  
129 that this spectrin stretching could, in part, account for the deformability changes of the iRBC (Dearnley  
130 et al., 2016), emphasizing the biological significance of the measurements. We sought to confirm these  
131 observations using a novel scanning electron microscopy (SEM)-based protocol (Blanch A. et al., in  
132 preparation). The method involves cross-linking the RBCs to a glass coverslip and shearing off the  
133 upper membrane component, thus exposing the cytoplasmic/internal side of the cross-linked plasma  
134 membrane (Shi et al., 2013). The membrane is chemically fixed, dehydrated and gold-coated before  
135 imaging (Figure 2A). We automatically extracted spectrin skeletons (Figure 2B) from images produced  
136 using both uninfected RBCs and RBCs infected with mature stage parasites (40-44h post infection). We  
137 found that the average spectrin branch distance increased from 45.5nm to 49.2nm, an increase of 8%  
138 (Figure 2C-D).

## 139 **DISCUSSION AND CONCLUSIONS**

### 140 **Spectrin remodelling by *P. falciparum***

141 The remarkable deformability and durability of the RBC membrane derives from its membrane skeleton  
142 (Zhang et al., 2015). The skeleton is composed of a regular hexagonal array of "spring-like" proteins

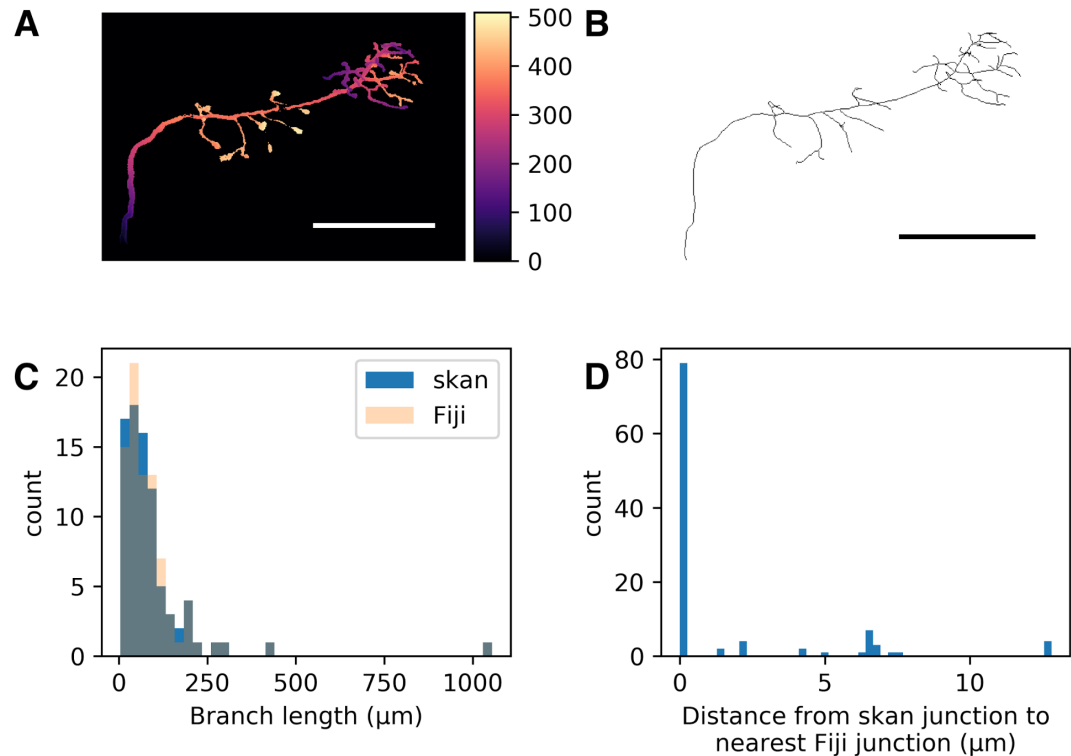


**Figure 1.** Comparison of skan and Fiji analysis results of the neuronal skeleton from olfactory projection neuron 1 (OP-1) from the DIADEM challenge. (A) Depth projection of the neuron. Scale bar: 500 $\mu$ m. Colour map: height in  $\mu$ m. (B) Skeleton of the neuron. (C) Distribution of 82 branch lengths between 103 branch points measured by Skan and Fiji in the neuronal skeleton. (D) Distance from 103 skan junction points to the nearest Fiji junction point. Note that the voxel spacing is approximately  $9 \times 3 \times 3 \mu$ m, so almost all of these distances are less than one pixel apart.

143 forming a meshwork at the cytoplasmic surface of the RBC. Spectrin heterodimers constitute the cross-  
 144 beams of the molecular architecture and are connected to integral membrane proteins in the plasma  
 145 membrane. Previous studies using atomic force microscopy (AFM) and transmission electron microscopy  
 146 (TEM), followed by manual selection and measurement of skeleton branches, revealed reorganization  
 147 and expansion of the spectrin network of the host cell membrane (Shi et al., 2013; Millholland et al.,  
 148 2011; Cyrklaff et al., 2011). In this work we have applied a novel SEM-based method to image the  
 149 RBC membrane skeleton, and a fully automated method for selection and measurement of the spectrin  
 150 branch distances. We observed an 8% increase in the length of the spectrin cross-members, in reasonable  
 151 agreement with previous studies. The data are consistent with a cryo-electron tomography study that  
 152 provided evidence that the RBC membrane skeleton is reorganised as a result of mining of the actin  
 153 junction points to generate actin filaments that connect parasite-derived organelles known as Maurer's  
 154 clefts to the knobs.

### 155 Numba and performance

156 An interesting aspect of Skan's development is its use of Numba, a just-in-time compiler for Python code.  
 157 Skan is one of the first scientific packages to make extensive use of Numba to speed up its operations.  
 158 In our hands, Numba has been able to dramatically speed up our code, in some cases approaching the  
 159 theoretical maximum performance of our CPUs.

160 As just one example, in the context of implementing Sauvola image thresholding, we developed a  
 161 function for the cross-correlation of an n-dimensional image with a sparse kernel. Sauvola thresholding  
 162 requires computing the local mean and standard deviation for every pixel in an image. This can be

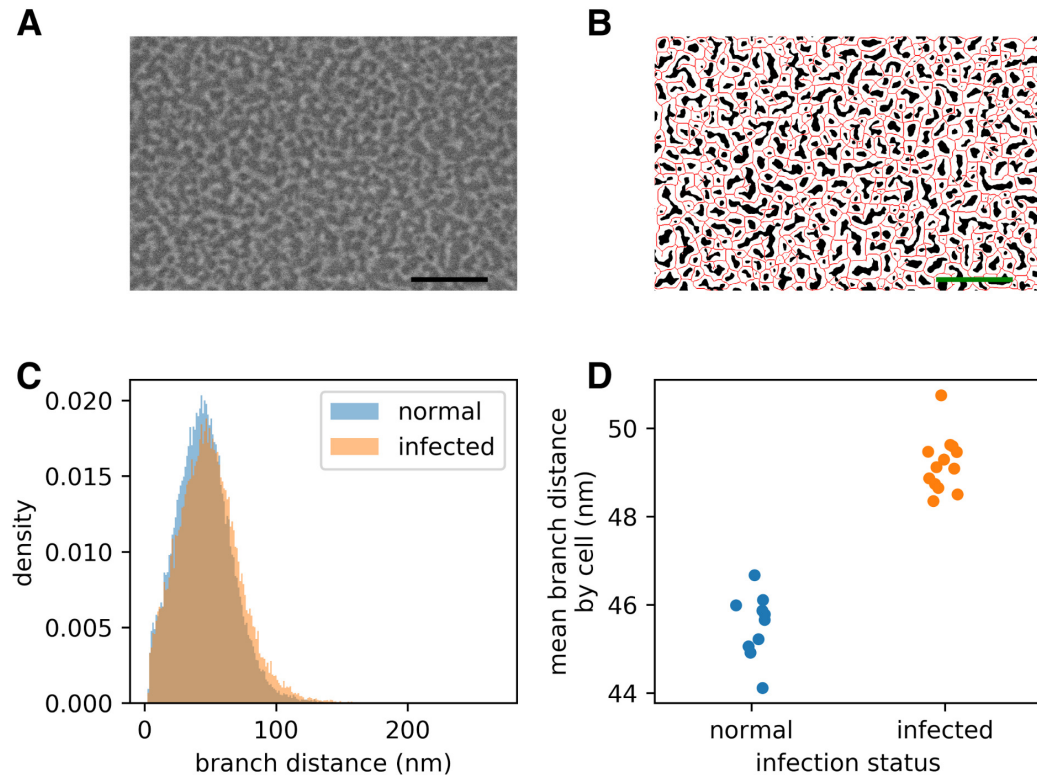


**Figure 2.** Infection by the malaria parasite remodels the spectrin skeleton of the host red blood cell in the asexual developmental stage. (A) Example image produced by our protocol. Scale bar: 300 nm. (B) Thresholding (white) and skeletonisation (red) of the image in (A). (C) Complete distribution of measured spectrin branch lengths for normal and infected RBCs. (D) Mean spectrin branch length by cell ( $n_{\text{norm}} = 10$ ,  $n_{\text{inf}} = 13$ ).

163 optimally achieved by computing the integral of both the original image and the image of squared  
 164 intensity values, and then convolving each with a kernel consisting of the outer product of the vector  
 165  $(-1, 0, 0, \dots, 0, 1)$  with itself, where the number of zeros is equal to the width of the neighbourhood minus  
 166 one. This definition results in an extremely sparse kernel, which is not efficiently used by conventional  
 167 convolution functions available in NumPy (v1.12) and SciPy (v0.19) (Walt et al., 2011; Oliphant, 2007).

168 The function is implemented as `correlate_sparse`, which handles boundary conditions and  
 169 formatting of the kernel, and then calls the Numba-jitted function `_correlate_sparse_offsets`,  
 170 which iterates through the array, performing the cross-correlation.

171 The result is striking. For a 2048 by 2048 pixel image and a 31 by 31 kernel size, `correlate_sparse`  
 172 takes 130ms, somewhat slower than SciPy's `ndimage.correlate`, which takes 57ms. For a much  
 173 bigger 301 by 301 kernel, however, `correlate_sparse` takes a similar amount of time — 135ms —  
 174 while SciPy takes 17s. Furthermore, if we analyse just the inner loop of the computation, the part handled  
 175 by Numba, we measured a time of 1.8ns per loop in our 1.3GHz (i.e. 0.77ns per cycle) CPU. Each loop  
 176 performs two additions and a multiplication, in addition to array access, suggesting that Numba is close to  
 177 achieving optimal performance for our problem and CPU. This example illustrates the power of Numba  
 178 to speed up numerical Python code.

179 We also take this opportunity to note the loop order in the code of `_correlate_sparse_offsets`.  
 180 For every non-zero element of the kernel, we make a full pass over the input image. When picturing a  
 181 convolution, this is slightly counter-intuitive: most people would instead consider, for each pixel position,  
 182 correlating all the non-zero elements of the kernel (thus examining each pixel only once).

183 However, that order of operations is poorly optimised for modern processor architectures, which  
 184 fetch RAM contents by chunks into the processor cache. Once a chunk has been loaded, access-

185 ing elements of that chunk is 20-200 times faster than fetching more data from RAM (Jonas Bonér,  
 186 <https://gist.github.com/jboner/2841832>). One consequence is that algorithms that access data in the order  
 187 in which it is stored in RAM end up being much faster, by virtue of using processor cache to the maximum  
 188 extent possible.

189 In our case, this translated to a 10-fold speedup when changing the order from (for pixel in  
 190 image: for elem in kernel) to (for elem in kernel: for pixel in image),  
 191 even though these two expressions are mathematically equivalent.

## 192 ACKNOWLEDGEMENTS

193 We thank Ignacio Arganda-Carreras for suggesting the dataset to compare Skan to Analyze Skeletons,  
 194 and Alan Rubin for help with Skan's GUI code.

195 This work was funded in part by Australian Research Council grant FL150100106.

## 196 REFERENCES

- 197 Arganda-Carreras, I., Fernández-González, R., Muñoz-Barrutia, A., and Ortiz-De-Solorzano, C. (2010).  
 198 3D reconstruction of histological sections: Application to mammary gland tissue. *Microsc. Res. Tech.*,  
 199 73(11):1019–1029.
- 200 Bas, E. and Erdogmus, D. (2011). Principal curves as skeletons of tubular objects. *Neuroinformatics*.
- 201 Cyrklaff, M., Sanchez, C. P., Kilian, N., Bisseye, C., Simporé, J., Frischknecht, F., and Lanzer, M. (2011).  
 202 Hemoglobins S and C interfere with actin remodeling in plasmodium falciparum-infected erythrocytes.  
 203 *Science*, 334(6060):1283–1286.
- 204 Dearnley, M., Chu, T., Zhang, Y., Looker, O., Huang, C., Klonis, N., Yeoman, J., Kenny, S., Arora, M.,  
 205 Osborne, J. M., Chandramohanadas, R., Zhang, S., Dixon, M. W. A., and Tilley, L. (2016). Reversible  
 206 host cell remodeling underpins deformability changes in malaria parasite sexual blood stages. *Proc.*  
 207 *Natl. Acad. Sci. U. S. A.*, 113(17):4800–4805.
- 208 Lam, S. K., Pitrou, A., and Seibert, S. (2015). Numba: A LLVM-based python JIT compiler. In  
 209 *Proceedings of the Second Workshop on the LLVM Compiler Infrastructure in HPC*, LLVM '15, pages  
 210 7:1–7:6, New York, NY, USA. ACM.
- 211 Longair, M. H., Baker, D. A., and Armstrong, J. D. (2011). Simple neurite tracer: open source software  
 212 for reconstruction, visualization and analysis of neuronal processes. *Bioinformatics*, 27(17):2453–2454.
- 213 Millholland, M. G., Chandramohanadas, R., Pizarro, A., Wehr, A., Shi, H., Darling, C., Lim, C. T.,  
 214 and Greenbaum, D. C. (2011). The malaria parasite progressively dismantles the host erythrocyte  
 215 cytoskeleton for efficient egress. *Mol. Cell. Proteomics*, 10(12):M111.010678.
- 216 Morales-Navarrete, H., Segovia-Miranda, F., Klukowski, P., Meyer, K., Nonaka, H., Marsico, G.,  
 217 Chernykh, M., Kalaidzidis, A., Zerial, M., and Kalaidzidis, Y. (2015). A versatile pipeline for  
 218 the multi-scale digital reconstruction and quantitative analysis of 3D tissue architecture. *Elife*, 4.
- 219 Nans, A., Mohandas, N., and Stokes, D. L. (2011). Native ultrastructure of the red cell cytoskeleton by  
 220 cryo-electron tomography. *Biophys. J.*, 101(10):2341–2350.
- 221 Oliphant, T. E. (2007). SciPy: Open source scientific tools for python. *Computing in Science and*  
 222 *Engineering*, 9:10–20.
- 223 Sambaer, W., Zatloukal, M., and Kimmer, D. (2011). 3D modeling of filtration process via polyurethane  
 224 nanofiber based nonwoven filters prepared by electrospinning process. *Chem. Eng. Sci.*, 66(4):613–623.
- 225 Sauvola, J. and Pietikäinen, M. (2000). Adaptive document image binarization. *Pattern Recognit.*,  
 226 33(2):225–236.
- 227 Shi, H., Liu, Z., Li, A., Yin, J., Chong, A. G. L., Tan, K. S. W., Zhang, Y., and Lim, C. T. (2013). Life  
 228 cycle-dependent cytoskeletal modifications in plasmodium falciparum infected erythrocytes. *PLoS*  
 229 *One*, 8(4):e61170.
- 230 Sundar, H., Silver, D., Gagvani, N., and Dickinson, S. (2003). Skeleton based shape matching and  
 231 retrieval. In *Shape Modeling International, 2003*, pages 130–139.
- 232 van der Walt, S., Schönberger, J. L., Nunez-Iglesias, J., Boulogne, F., Warner, J. D., Yager, N., Gouillart,  
 233 E., Yu, T., and scikit-image contributors (2014). scikit-image: image processing in python. *PeerJ*,  
 234 2:e453.
- 235 Walt, S. v. d., Colbert, S. C., and Varoquaux, G. (2011). The NumPy array: A structure for efficient  
 236 numerical computation. *Comput. Sci. Eng.*, 13(2):22–30.

- 237 Wickham, H. (2014). Tidy data. *J. Stat. Softw.*, 59(10).
- 238 Yim, P. J., Choyke, P. L., and Summers, R. M. (2000). Gray-scale skeletonization of small vessels in  
239 magnetic resonance angiography. *IEEE Trans. Med. Imaging*, 19(6):568–576.
- 240 Yuan, X., Trachtenberg, J. T., Potter, S. M., and Roysam, B. (2009). MDL constrained 3-D grayscale  
241 skeletonization algorithm for automated extraction of dendrites and spines from fluorescence confocal  
242 images. *Neuroinformatics*, 7(4):213–232.
- 243 Zhang, T. Y. and Suen, C. Y. (1984). A fast parallel algorithm for thinning digital patterns. *Commun.*  
244 *ACM*, 27(3):236–239.
- 245 Zhang, Y., Huang, C., Kim, S., Golkaram, M., Dixon, M. W. A., Tilley, L., Li, J., Zhang, S., and Suresh,  
246 S. (2015). Multiple stiffening effects of nanoscale knobs on human red blood cells infected with  
247 plasmodium falciparum malaria parasite. *Proc. Natl. Acad. Sci. U. S. A.*, 112(19):6068–6073.

## 248 SUPPLEMENTARY RESULTS

### 249 Pixel-level comparison with Analyze Skeletons

250 Although the results obtained by our software are broadly similar to those of Analyze Skeletons, we  
251 investigated the behaviour of both tools on a tiny example image, to ensure that we understood the minor  
252 discrepancies between the two.

253 The differences between the libraries occur in the handling of clusters of junction nodes. It is  
254 impossible to guarantee that several branches of a skeleton will converge on a single “junction” pixel. For  
255 example, Supplementary Figure 1A shows a fully-reduced skeleton of 10 pixels. Counting the number of  
256 neighbours of each pixel, we classify pixels as end-points, paths, and junctions. However, we can see that  
257 four contiguous pixels at the bottom-centre are all considered junctions (Supplementary Figure S1B-C).  
258 We saw three possible ways to deal with such clusters when computing branch statistics:

- 259 1. Ignore them — the branch from pixel 1 to pixel 3 will be considered to have length 2, as will the other  
260 branches; the junction clusters are thus considered to have some “spatial extent.” (Supplementary  
261 Figure S1D)
- 262 2. Replace them by a single pixel, perhaps the pixel closest to the centroid of the pixels.
- 263 3. Replace them by their centroid. (Supplementary Figure S1E)

264 In Skan, we added a flag, `unique_junctions`, that selects between options 1 and 3. The Analyze  
265 Skeletons plugin, in contrast, uses a variant of option 2, where the pixel selected to represent the cluster is  
266 the “earliest,” in lexicographical order of (x, y[, z]) position (Supplementary Figure S1F). We believe our  
267 approach is more representative of what a user would prefer to know about their skeleton images.

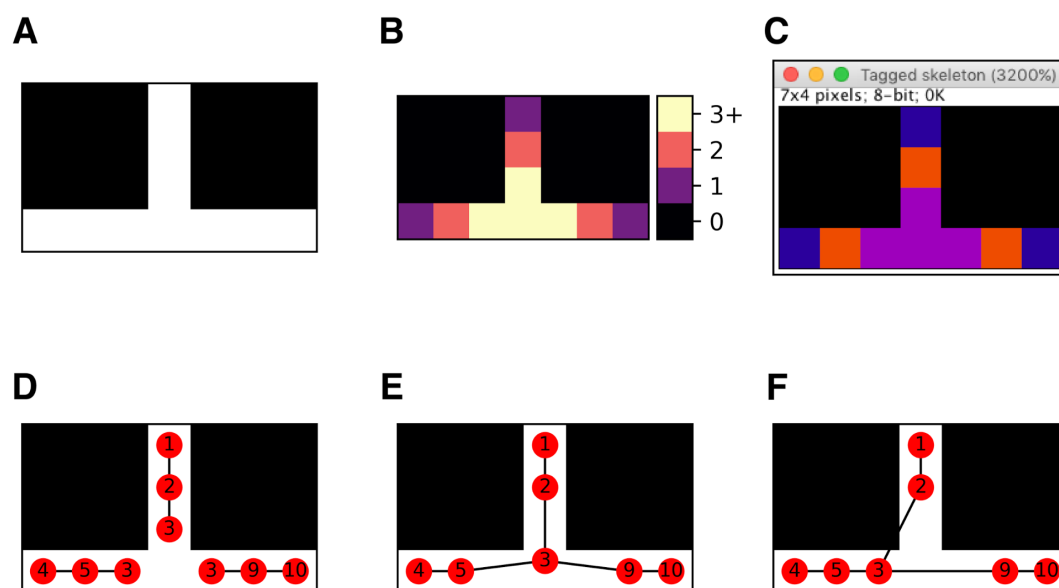


**Figure S1.** Strategies for resolving skeleton junctions. (A) A minimal skeleton. (B) Skan's classification of pixels into endpoints, paths, and junctions based on the number of neighbours (1, 2, and 3 or more, respectively). (C) Identical classification in Fiji's Analyze Skeletons. (D) Skeleton measurement when junctions are assigned an implicit "extent". (E) Skeleton measurement when all adjacent junction pixels are replaced by their centroid (our default strategy). (F) Skeleton measurement used in Fiji's Analyze skeletons (mid-2017 version).